

1 **On the barium - oxygen consumption relationship in the Mediterranean Sea: implications**
2 **for mesopelagic marine snow remineralisation.**

3

4 Stéphanie H.M. Jacquet^{1*}, Dominique Lefèvre¹, Christian Tamburini¹, Marc Garel¹, Frédéric
5 A.C. Le Moigne¹, Nagib Bhairy¹, Marie Roumagnac¹, Sophie Guasco¹

6

7 ¹Aix Marseille Université, CNRS/INSU, Université de Toulon, IRD, Mediterranean Institute of
8 Oceanography (MIO), UM 110, 13288 Marseille, France.

9

10 *Correspondence to: S. Jacquet (*stephanie.jacquet@mio.osupytheas.fr*)

11

12

13 Biogeosciences

14

15

16

17

18 **ABSTRACT**

19 In the ocean, remineralisation rate associated with sinking particles is a crucial variable. Since
20 the 90's, particulate biogenic barium (Ba_{xs}) has been used as an indicator of carbon
21 remineralization by applying a transfer function relating Ba_{xs} to O_2 consumption (Dehairs's
22 transfer function, Southern Ocean-based). Here, we tested its validity in the Mediterranean Sea
23 (ANTARES / EMSO-LO) for the first time by investigating connections between Ba_{xs} ,
24 prokaryotic heterotrophic production (PHP) and oxygen consumption (JO_2 -Opt; optodes
25 measurement). We show that: (1) higher Ba_{xs} (409 pM; 100- 500 m) occurs in situations where
26 integrated PHP ($PHP_{100/500} = 0.90$) is located deeper, (2) higher Ba_{xs} occurs with increasing
27 JO_2 -Opt, and (3) similar magnitude between JO_2 -Opt ($3.14 \text{ mmol m}^{-2} \text{ d}^{-1}$; 175- 450 m) and JO_2 -
28 Ba ($4.59 \text{ mmol m}^{-2} \text{ d}^{-1}$; transfer function). Overall, Ba_{xs} , PHP and JO_2 relationships follow trends
29 observed earlier in the Southern Ocean. We conclude that such transfer function could apply in
30 the Mediterranean Sea.

31
32
33 **KEY WORDS:** particulate biogenic barium, mesopelagic zone, oxygen consumption,
34 prokaryotic heterotrophic production, carbon remineralization, Mediterranean Sea

35

36 1. INTRODUCTION

37 Ocean ecosystems play a critical role in the Earth's carbon (C) cycle [IPCC, 2014]. The
38 quantification of their impacts of both present conditions and future predictions remains one of
39 the greatest challenges in oceanography [Siegel et al., 2016]. In essence, the biological C pump is
40 termed for the numerous processes involved in maintaining the vertical gradient in dissolved
41 inorganic C. This includes processes such as organic matter production in surface, its export and
42 subsequent remineralization. Most of marine snow organic C conversion (i.e. remineralization)
43 into CO₂ by heterotrophic organisms (i.e. respiration) occurs in the mesopelagic zone (100-1000
44 m) [Martin et al., 1987; Buesseler and Boyd, 2009]. Globally, the flux of C exported below 1000
45 m depth is the key determinant of ocean carbon storage capacity [Henson et al., 2011]. However,
46 there is no consensus on C transfer efficiency estimations from field experiments, leading to an
47 imbalance of the water column C budget [Giering et al., 2014]. Resolving this imbalance is in the
48 core of numerous studies in the global ocean, but also regionally, especially in the Mediterranean
49 Sea (MedSea). Due to limited exchanges with adjacent basin and the existence of an intense
50 overturning circulation qualitatively resembling the global one (but with shorter time scales), the
51 MedSea is often considered as a laboratory to observe and understand the impact of transient
52 climate variability on ecosystems and biogeochemical cycles [Malanotte-Rissoli et al., 2014]. In a
53 context of climate changes, better constraining C fluxes and the ocean C storage capacity is of
54 crucial importance.

55 Particulate barium in excess (Ba_{xs}, i.e. biogenic Ba from total particulate Ba after correction for
56 lithogenic Ba) is a geochemical tracer of particulate organic carbon (POC) remineralization in the
57 mesopelagic layer [Dehairs et al., 1997]. Ba_{xs} mostly occurs in the form of barite microcrystals
58 (BaSO₄) at these depths. In a global ocean undersaturated with respect to barite, studies report
59 that Ba_{xs} would precipitate inside oversaturated biogenic micro-environments during POC

60 degradation by heterotrophic prokaryotes in the mesopelagic zone, through sulfate and/or barium
61 enrichment [Bertram and Cowen, 1997]. The first-ever studies on mesopelagic Ba_{xs} reported
62 coinciding Ba_{xs} maxima with depths of dissolved O_2 minimum and pCO_2 maximum [Dehairs et
63 al., 1987, 1997]. By using an 1D advection-diffusion model applied to O_2 profiles in the Atlantic
64 sector of the Southern Ocean (ANTX/6 cruise; Shopova et al., 1995), Dehairs et al. [1997]
65 established an algorithm converting mesopelagic Ba_{xs} concentration into O_2 consumption rate
66 (JO_2) and organic C remineralized (POC remineralization rate). This transfer function has been
67 widely used until now [Cardinal et al., 2001, 2005; Dehairs et al., 2008; Jacquet et al., 2008a,
68 2008b, 2011, 2015]. Yet its validity has never been tested in other oceanic provinces. In the
69 North Atlantic, Lemaitre et al. [2018] reported a Ba_{xs} - JO_2 (obtained from apparent oxygen
70 utilisation divided by the water mass age) relationship not significantly different to that reported
71 in Dehairs et al. [1997]. Furthermore, significant progresses were made in relating Ba_{xs} , O_2
72 dynamics to prokaryotic heterotrophic activity [Jacquet et al., 2015]. These advancements clearly
73 show that Ba_{xs} is closely related with the vertical distribution of prokaryotes heterotrophic
74 production (PHP) (the rate of change with depth), reflecting the temporal progression of POC
75 remineralization processes. Also, in a first attempt to test the validity of the Dehairs's transfer
76 function in other locations, Jacquet et al. [2015] confronted oxygen consumption rates (JO_2) from
77 direct measurements (dark community respiration, DCR) to derived JO_2 from Ba_{xs} data (using the
78 transfer function) in the Kerguelen area (Indian sector of the Southern Ocean). We revealed good
79 convergence of JO_2 rates from these two approaches, further supporting the Dehairs's function to
80 estimate POC remineralization rates in different biogeochemical settings of the Southern Ocean.

81 Here, we further investigate relationships between the mesopelagic Ba_{xs} proxy, prokaryotic
82 activity and oxygen dynamics (Figure 1a) in the northwestern Mediterranean Sea (MedSea), a
83 different biogeochemical setting to those already studied (see references above). Today,

84 observations of the various components of the MedSea biological C pump provide organic C
85 [rem mineralization](#) fluxes varying by at least an order of magnitude [Santinelli et al., 2010;
86 Ramondenc et al., 2016]. Malanotte-Rissoli et al. [2014] reviewing unsolved issues and future
87 directions for MedSea research highlighted the need to further investigate biogeochemical
88 processes at intermediate (mesopelagic) and deep layers to reconcile the C budget in the
89 Mediterranean basin. Previous particulate Ba_{xs} dataset is very scarce in the NW- MedSea, with in
90 general very low vertical sampling resolution [Sanchez Vidal et al., 2005] or very restricted
91 studied areas [Dehairs et al., 1987; Sternberg et al., 2008]. Here we discuss Ba_{xs} , PHP and JO_2
92 (from optodes measurement during incubations) at the ANTARES / EMSO-LO observatory site
93 (Figure 1a, b). We hypothesize that the Dehairs's transfer function converting Ba_{xs} into POC
94 remineralization also applies in a different ocean ecosystem functioning from the Southern
95 Ocean. We suggest that the Ba_{xs} proxy can be used as routine tracer to estimate local-scale
96 processes of mesopelagic POC remineralization in the Mediterranean basin.

97

98 | **2. [METHODS](#)**

99 | **2.1 STUDY SITE**

100 The BATMAN cruise (<https://doi.org/10.17600/16011100>, March 10-16 2016, *R/V EUROPE*)
101 took place to the ANTARES / EMSO-LO observatory site (42°48'N, 6°10'E; Tamburini et al.,
102 2013), 40 km off the coast of Toulon, southern France (Figure 1b). The hydrological and
103 biogeochemical conditions at this site are monitored monthly in the framework of the MOOSE
104 (Mediterranean Ocean Observing System for the Environment) program and of the EMSO
105 (European Multidisciplinary Subsea Observatory) observation program. The hydrography
106 displays the general three-layer MedSea system with surface, intermediate and deep waters
107 [Hainbucher et al., 2014]. Briefly, the main water masses can be distinguished (see potential

108 temperature – salinity diagram during the BATMAN cruise in Figure 1c): (1) Surface Water
109 (SW); (2) Winter Intermediate Water (WIW); (3) Levantine Intermediate water (LIW). LIW is
110 present at intermediate depths (around 400 m at ANTARES) and is characterized by temperature
111 and a salinity maxima; (4) Mediterranean Deep Water (MDW).

112

113 **2.2 SAMPLING AND ANALYSES**

114 For particulate barium, 4 to 7 L of seawater sampled using Niskin bottles were filtered onto 47
115 mm polycarbonate membranes (0.4 μm porosity) under slight overpressure supplied by filtered
116 air. Filters were rinsed with few mL of Milli-Q grade water to remove sea salt, dried (50°C) and
117 stored in Petri dishes. Thirteen depths between surface and 1000 m were sampled by combining
118 different casts sampled closely in time and space (total of 28 samples) with similar potential
119 temperature – salinity profiles. No major changes in water mass characteristics occurred over the
120 3-day sampling period (Figure 1c). In the laboratory, we performed a total digestion of filters
121 using a concentrated tri-acid (0.5 mL HF /1.5 mL HNO₃ / HCl 1 mL; all Optima grade) mixture
122 in closed teflon beakers overnight at 95°C in a clean pressurized room. After evaporation close to
123 dryness, samples were re-dissolved into 10 mL of HNO₃ 2%. The solutions were analysed for Ba
124 and other elements of interest (Na and Al) by HR-ICP-MS (High Resolution-Inductively Coupled
125 Plasma- Mass Spectrometry; ELEMENT XR ThermoFisher). Based on analyses of external
126 certified reference standards, accuracy and reproducibility were both within $\pm 5\%$. Details on
127 sample processing and analysis are given in Cardinal et al. [2001] and Jacquet et al. [2015]. The
128 presence of sea-salt was checked by analysing Na and the sea-salt particulate Ba contribution was
129 found negligible (<0.1% of total Ba). Particulate biogenic barium in excess (hereafter referred to
130 as Ba_{xs}) was calculated as the difference between total Ba and lithogenic Ba using Al as the
131 lithogenic reference element. The lithogenic Ba concentration was determined using Al

132 [concentration and the upper continental crust \(UCC\) Ba:Al molar ratio \[Taylor and Mc.Lennan,](#)
133 [1985\]. The biogenic Ba fraction ranged from 51 to 91 % of the total particulate Ba signal \(see](#)
134 [below\).](#) The standard uncertainty [Ellison et al., 2000] on Ba_{xs} concentration ranges between 5.0
135 and 5.5%. The term “in excess” is used to indicate that concentrations are larger than the Ba_{xs}
136 background. The background (or residual value) is considered as “preformed” Ba_{xs} at zero
137 oxygen consumption left over after transfer and partial dissolution of Ba_{xs} produced during
138 degradation of previous phytoplankton growth events. [The background is set at 130 pM in this](#)
139 [study.](#)

140 [Oxygen concentrations were measured using oxygen optode Aanderaa® 4330 for at least 24](#)
141 [hours \(on a 30 seconds time step\) on samples taken at 4 depths in the mesopelagic layer \(175,](#)
142 [250, 450 and 1000 m\). Samples were placed into a sealed 1L borosilicate glass bottles incubated](#)
143 [at a constant temperature of 13°C in thermo-regulated baths. Optodes were calibrated using a](#)
144 [home made calibration facility \(\[https://www.mio.osupytheas.fr/en/cybele/oxygen-dynamics-\]\(https://www.mio.osupytheas.fr/en/cybele/oxygen-dynamics-construction-oxygen-optode-calibration-platform\)](#)
145 [construction-oxygen-optode-calibration-platform\).](#) Oxygen consumption rates (later referred to as
146 JO₂-Opt) were derived from a linear model calculation. Associated errors to the linear model fit
147 are below 0.01 μM O₂ h⁻¹. Each oxygen consumption experiment has been duplicated for each
148 depth. Average and standard deviation of the duplicates are reported in Fig 3a. The larger
149 associated errors are related to the differences between each duplicates, especially in surface,
150 reflecting potential heterogeneity of the microbial community during sampling.

151 Prokaryotic heterotrophic production (PHP) estimation was measured over time course
152 experiments at *in situ* temperature (13°C) following the protocol described in Tamburini et al.
153 [2002]. ³H-leucine labelled tracer [Kirchman, 1993] was used. To calculate prokaryotic
154 heterotrophic production, we used the empirical conversion factor of 1.55 ng C per pmol of

155 incorporated leucine according to Simon and Azam [1989], assuming that isotope dilution was
156 negligible under these saturating concentrations.

157

158 **3. RESULTS AND DISCUSSION**

159 **3.1 Particulate Ba_{xs} vertical distribution**

160 Particulate biogenic Ba_{xs}, particulate Al (pAl) and biogenic Ba fraction profiles in the upper
161 1000 m at ANTARES are reported in Figure 2a. Ba_{xs} concentrations range from 12 to 719 pM.

162 The biogenic Ba fraction ranges from 51 to 91 % of the total particulate Ba signal. Particulate Al
163 concentrations (pAl) range from 8 to 170 nM. Ba_{xs} concentrations are low in surface water (<100

164 pM) where the lithogenic fraction reaches 43 to 49 % in the upper 70 m. From previous studies

165 we know that Ba_{xs} in surface waters is distributed over different, mainly non-barite biogenic

166 phases, and incorporated into or adsorbed onto phytoplankton material. As such these do not

167 reflect POC remineralization processes, in contrast to mesopelagic waters where Ba_{xs} is mainly

168 composed of barite formed during prokaryotic degradation of organic matter. At ANTARES the

169 Ba_{xs} profile displays a mesopelagic Ba_{xs} maximum between 100 and 500 m, reaching up to 719

170 pM at 175 m. Ba is mostly biogenic at these depths (> 80 %). Ba_{xs} concentrations then decrease

171 below 500 m to reach a background value of around 130 pM (see BKG in Figure 2). Note that the

172 MedSea is largely undersaturated with respect to barite, with saturation state ranging between 0.2

173 and 0.6 over the basin [Jacquet et al., 2016; Jullion et al., 2017]. For comparison, the Ba_{xs}

174 background value in the Southern Ocean reaches 180 to 200 pM below 1000 m [Dehairs et al.,

175 1997; Jacquet et al. 2015]. Previously, Sternberg et al. [2008] reported the seasonal evolution of

176 Ba_{xs} profiles at the DYFAMED station (43°25'N-7°52'E; BARMED project) northeast from

177 ANTARES (Figure 1c) in the NW-MedSea. The present Ba_{xs} profile at ANTARES (March 2016)

178 is very similar to the Ba_{xs} profile measured in March 2003 at DYFAMED (Figure 2a). The slight

179 difference between Ba_{xs} profiles in the upper 75 m suggests more Ba bounded and/or adsorbed
180 onto phytoplankton material during BARMED. Both profiles present a Ba_{xs} maximum in the
181 upper mesopelagic zone between 150 and 200 m. Below this maximum, Ba_{xs} concentrations
182 gradually decrease to reach around 130 pM between 500 and 1000 m (this study). A similar value
183 was reached between 500 and 600 m at the DYFAMED station over the whole studied period
184 (between February and June 2003; Sternberg et al., 2008).

185

186 **3.2 Prokaryotic heterotrophic production**

187 The particulate Ba [in excess](#) is centred in the upper mesopelagic zone between 100 and 500 m
188 and reflects that POC remineralization mainly occurred at [this depth layer](#) (Figure 2a). Depth-
189 weighted average (DWA) Ba_{xs} content (409 pM), [i.e. the \$Ba_{xs}\$ inventory divided by the depth](#)
190 [layer considered](#), was calculated [between 100 and 500 m](#). Figure 2b shows [the](#) column-integrated
191 PHP at 100 m over [the one](#) at 500 m (PHP100/500). [Our PHP100/500 ratio at ANTARES station](#)
192 [is of 0.90 and is compared to results](#) obtained during KEOPS1 (summer) and KEOPS2 (spring;
193 out plateau stations) cruises in the Southern Ocean [Jacquet et al., 2008; 2015] and #DY032
194 cruise ([July 2015, R/V DISCOVERY](#)) at the PAP (Porcupine Abyssal Plain) observatory in the
195 northeast Atlantic (49°N, 16.5 °W) (personal data). Result at the ANTARES / EMSO-LO site
196 follows the trend previously reported in the Southern Ocean ([blue line in Figure 2b; Jacquet et al.,](#)
197 [2015](#)), indicating higher DWA Ba_{xs} in situations where a significant part of column-integrated
198 PHP is located deeper in the water column (high Int. PHPx1/IntPHPx2 ratio; Figure 2b). These
199 previous studies revealed that the shape of the column-integrated PHP profile (i.e. the attenuation
200 gradient) is important in setting the Ba_{xs} signal in the mesopelagic zone (Dehairs et al., 2008;
201 Jacquet et al., 2008, 2015]. Indeed, mesopelagic [DWA](#) Ba_{xs} appears reduced when most of the
202 column-integrated PHP is limited to the upper layer, [i.e.](#) indicating an efficient remineralization

203 in surface. In contrast, mesopelagic DWA Ba_{xs} appears higher when most of the column-
204 integrated PHP is located in the mesopelagic layer, i.e. reflecting significant deep PHP activity,
205 POC export and subsequent remineralization (Figure 2b). Results at the PAP site reflect a similar
206 situation as observed during KEOPS2 for time series stations at Plateau site and in a meander of
207 the polar front area (not show in Figure 2b). At these stations, Jacquet et al. [2015] reported a
208 shift toward the KEOPS1 trend reflecting the temporal evolution (season advancement) and
209 patchiness of the establishment of mesopelagic remineralization processes within a same area.
210 Overall, our MedSea result is located along the trend defined in the Southern Ocean during
211 KEOPS1 cruise. It is generally considered that Ba_{xs} (barite) forms inside sulfate and/or barium
212 oversaturated biogenic micro-environments during POC degradation by heterotrophic
213 prokaryotes. However, it is unclear whether barite formation at mesopelagic depths is (directly or
214 indirectly) bacterially induced or bacterially influenced [Martinez-Ruiz et al., 2018, 2019]. In any
215 case our results strengthen the close link between the water column Ba_{xs} distribution and
216 respiration (organic matter degradation).

217

218 **3.3 Oxygen- barium relationship**

219 The relationship we obtained at ANTARES between Ba_{xs} concentrations and oxygen
220 consumption rates from optodes measurements (JO_2 -Opt) is reported in Figure 3a. JO_2 -Opt range
221 from 0.11 to 5.85 $\mu\text{mol L}^{-1} \text{d}^{-1}$. The relationship indicates higher Ba_{xs} concentrations with
222 increasing JO_2 -Opt. An interesting feature is the intercept at zero JO_2 -Opt (around 128 pM)
223 which further supports the Ba BKG value at ANTARES (130 pM) determined from measured
224 Ba_{xs} profiles (Figure 3a).

225 In figure 3b we applied a similar approach as reported in Jacquet et al. [2015] where we show
226 the correlation between JO_2 obtained from dark community respiration DCR (Winkler titration;

227 JO₂-DCR) data integration in the water column and JO₂ based on Ba_{xs} content (Dehairs's transfer
228 function; later referred to as JO₂-Ba). Similarly, to estimate JO₂-Ba in the present study we used
229 the following equation [Dehairs et al., 1997] (Figure 3c):

$$230 \quad \text{JO}_2\text{-Ba} = (\text{Ba}_{\text{xs}} - \text{Ba BKG}) / 17450 \quad (1)$$

231 A Ba BKG value of 130 pM was used (see above). JO₂-Ba is confronted to JO₂-Opt integrated
232 over the same layer depth (between 175 and 450 m; Figure 3b). JO₂ rates are of the same order of
233 magnitude (JO₂-Ba= 4.59 mmol m⁻² d⁻¹ and JO₂-opt= 3.14 mmol m⁻² d⁻¹). The slight difference
234 could be explained by the integration time of both methods: few hours to days for the incubations
235 vs. few days to weeks for Ba_{xs} (seasonal build-up; Jacquet et al., 2007). JO₂ rates calculated in the
236 present work are 3 times higher than those reported in the Southern Ocean during KEOPS1
237 [Jacquet et al., 2015] but they are in good agreement with the Ba_{xs} vs JO₂ trend (Figure 3b).
238 [DWA Ba_{xs} and JO₂ measured during KEOPS1 \[Jacquet et al., 2015\] and at ANTARES site \(this](#)
239 [study\) are compared to Dehairs's relationship in Figure 3c. The correlation obtained in Lemaitre](#)
240 [et al. \[2018\] in the North Atlantic is also reported \(JO₂ were calculated from apparent oxygen](#)
241 [utilisation divided by water mass age\). Note that this relationship is not significantly different](#)
242 [from the Dehairs's equation \[Lemaitre et al., 2018\]. Overall, results at the ANTARES site are](#)
243 [lying along the Southern Ocean Ba_{xs} - JO₂ correlation.](#) This further supports the validity of the
244 Dehairs's transfer function in the present study.

245

246 **3.4 Estimated particles remineralisation rates and implications**

247 In order to provide a Ba_{xs}-derived estimate of POC remineralization rate (MR) at the
248 ANTARES / EMSO-LO observatory during BATMAN cruise, we converted JO₂-Ba into C
249 respired using the Redfield (RR) C/O₂ molar ratio (127/175; Broecker et al., 1985) multiplied by
250 the depth layer considered (Z, [175-450 m](#)) [Dehairs et al., 1997]:

$$MR = Z \times JO_2 - Ba \times RR \quad (2)$$

We obtain a POC remineralization rate of $11 \text{ mmol C m}^{-2} \text{ d}^{-1}$ (10% RSD). This is within the range of dissolved Ba- derived fluxes of POC remineralization (13 to $29 \text{ mmol C m}^{-2} \text{ d}^{-1}$) reported in the Mediterranean Sea previously [Jacquet et al., 2016; Jullion et al., 2017]. Following calculations reported in Jullion et al. [2007], our MR rate would correspond to a Ba_{xs} flux of around $0.01 \text{ } \mu\text{mol m}^{-2} \text{ d}^{-1}$. This is in reasonable agreement with barium fluxes (0.01 to $0.08 \text{ } \mu\text{mol m}^{-2} \text{ d}^{-1}$) presented in Jullion et al. [2007]. Previously published barium fluxes from sediment trap range from 0.27 to $0.36 \text{ } \mu\text{mol m}^{-2} \text{ d}^{-1}$ at the DYFAMED station [Sternberg et al., 2007] and from 0.39 to $1.07 \text{ } \mu\text{mol m}^{-2} \text{ d}^{-1}$ in the Alboran Sea [Sanchez-Vidal et al., 2005]. POC remineralization rate from the present study is in the range of previously published carbon export fluxes (few to tens $\text{mmol m}^{-2} \text{ d}^{-1}$) from thorium-derived data [Speicher et al., 2006] or from combining drifting sediment traps and underwater vision profilers [Ramondenc et al., 2016]. Constraining POC flux attenuation and remineralization rates in the Mediterranean is far from being achieved, but the concordance of the different approaches is promising.

4. CONCLUSIONS

The present paper brings a first insight into the connections of Ba_{xs} , PHP and JO_2 at the ANTARES/EMSO-LO observatory site in the northwestern Mediterranean Sea during the BATMAN (2016) cruise. Our results reveal a strong relationship between Ba_{xs} contents and measured JO_2 rates. Also, DWA Ba_{xs} vs. column integrated PHP, as well as measured vs. Ba_{xs} -based JO_2 relationships follow trends previously reported in the Southern Ocean where the Dehairs's function was first established to estimate POC remineralisation rate. Results from the present study would indicate that this function can also be applied in the Mediterranean basin provided that adequate Ba_{xs} background values are estimated. From a global climate perspective,

275 the Ba_{xs} tool will help to better balance the MedSea water column C budget. It will contribute to
276 gain focus on the emerging picture of the C transfer efficiency (strength of the biological pump).

277

278 DATA AVAILABILITY

279 All data and metadata will be made available at the French INSU/CNRS LEFE CYBER
280 database (scientific coordinator: Hervé Claustre; data manager, webmaster: Catherine
281 Schmechtig). INSU/CNRSLEFE CYBER (2020)

282

283 AUTHOR CONTRIBUTION

284 SJ and DL designed the experiment for JO₂. SJ, CT and MG designed the experiments for PHP
285 measurements. SJ and FLM managed barium sampling during the cruise. NB managed CTD
286 deployment at sea. MG, SG and MR managed PHP. All co-authors contributed to writing.

287

288 COMPETING INTERESTS

289 The authors declare that they have no known competing financial interests or personal
290 relationships that could have appeared to influence the work reported in this paper.

291

292 **ACKNOWLEDGEMENTS**

293 We thank the officers and crew of *R/V EUROPE* for their assistance during work at sea. This
294 research was supported by the French national LEFE/INSU “REPAP” project (PI. S. Jacquet). It
295 was co-funded by the “ROBIN” project (PIs. C. Tamburini, F.A.C. Le Moigne) of Labex OT-
296 Med (ANR-11-LABEX-0061) funded by the Investissements d’Avenir and the French
297 Government project of the ANR, through the A*Midex project (ANR-11-IDEX-0001-02).
298 Authors have benefited of the support of the SNO-MOOSE and SAM-MIO. BATMAN is a
299 contribution to the "AT – POMPE BIOLOGIQUE" of the Mediterranean Institute of
300 Oceanography (MIO) and to the international IMBER program. The instrument (ELEMENT XR,
301 ThermoFisher) was supported in 2012 by European Regional Development Fund (ERDF).

303 **Figure captions**

304 Figure 1: (a) Schematic representation of the convergence of the different estimators of oxygen
305 consumption and C remineralization rates from the “oxygen dynamics”, “barium proxy” and
306 “prokaryotic activity” tools; (b) Location of the BATMAN cruise at the ANTARES observatory
307 site in the NW-Mediterranean Sea (42°48’N, 6°10’E). [The location of the DYFAMED station is](#)
308 [reported for comparison \(Sternberg et al., 2008\)](#); (c) Potential temperature - salinity - depth plots
309 and isopycals for BATMAN profiles. SW : Surface Water, WIW : Winter Intermediate Water,
310 LIW : Levantine Intermediate Water, DMW : Deep Mediterranean Water. Graph constructed
311 using Ocean Data View (Schlitzer, 2002; Ocean Data View; [http://www.awi-
312 bremerhaven.de/GEO/ODV](http://www.awi-
312 bremerhaven.de/GEO/ODV))

313
314 Figure 2: (a) Particulate biogenic Ba_{xs} (pM) and particulate Al (nM) profiles next to the biogenic
315 Ba fraction (%) in the upper 1000 m at ANTARES. The grey area represents a biogenic Ba
316 fraction larger than 80 %. BKG: Ba_{xs} background. Ba_{xs} profile (pM) at DYFAMED : data [from](#)
317 [Sternberg et al. \(2008\)](#); (b) ANTARES ratio plot (green square) of integrated PHP in the upper
318 100 m over integrated PHP in the upper 500 m versus depth-weighted average (DWA)
319 mesopelagic Ba_{xs} (pM) over the [100-500m](#) depth interval. Regression of the same ratio is
320 reported for KEOPS1 ([light blue symbols](#); out plateau stations) and KEOPS2 ([dark blue symbols](#);
321 [Southern Ocean, Jacquet et al., 2015](#)) and #DY032 ([red square](#); PAP station, NE-Atlantic; pers.
322 data) cruises. [The blue line represents the trend obtained during KEOPS2 \(Jacquet et al., 2015\).](#)

323
324 Figure 3: (a) Relationship between Ba_{xs} concentrations (pM) and oxygen consumption rates
325 ($\mu\text{mol L}^{-1} \text{d}^{-1}$) from optodes measurements (JO₂-Opt) at ANTARES; (b) Confrontation of oxygen
326 consumption rates ([JO₂](#); $\text{mmol m}^{-2} \text{d}^{-1}$) obtained from different methods: optodes measurements

327 (this [study; green square](#)) and dark community respiration DCR (winkler titration; [red triangles](#);
328 JO_2 -DCR; Jacquet et al., 2015; KEOPS1), and Dehairs's transfer function calculation ([Dehairs et](#)
329 [al., 1997](#)) based on Ba_{xs} contents. The black line corresponds to the correlation obtained during
330 [KEOPS1 \(Jacquet et al., 2015\)](#); (c) Dehairs's relationship between depth-weighted average
331 (DWA) mesopelagic Ba_{xs} (pM) and JO_2 ($\mu\text{mol L}^{-1} \text{d}^{-1}$) compared to ANTARES result (this
332 [study](#)), [KEOPS1 data \(Southern Ocean; Jacquet et al., 2015\)](#) and [GEOVIDE correlation \(North](#)
333 [Atlantic; Lemaitre et al., 2018\)](#).

334

335 **References**

336 Bertram, Miriam, and James P. Cowen. “Morphological and Compositional Evidence for Biotic
337 Precipitation of Marine Barite.” *Journal of Marine Research* 55 (1997): 577–93.

338 Broecker, Wallace S. “‘NO’, a Conservative Water-Mass Tracer.” *Earth and Planetary Science
339 Letters* 23, no. 1 (August 1974): 100–107. doi:10.1016/0012-821X(74)90036-3.

340 Buesseler, Ken O., and Philip W. Boyd. “Shedding Light on Processes That Control Particle
341 Export and Flux Attenuation in the Twilight Zone of the Open Ocean.” *Limnology and
342 Oceanography* 54, no. 4 (2009): 1210–32. doi:10.4319/lo.2009.54.4.1210.

343 Cardinal, Damien, Frank Dehairs, Thierry Cattaldo, and Luc André. “Geochemistry of Suspended
344 Particles in the Subantarctic and Polar Frontal Zones South of Australia: Constraints on
345 Export and Advection Processes.” *Journal of Geophysical Research: Oceans* 106, no. C12
346 (décembre 2001): 31637–56. doi:10.1029/2000JC000251.

347 [Cardinal D., Savoye N., Trull T. W., André L., Kopczynska E. E., and Dehairs F.: Variations of
348 carbon remineralisation in the Southern Ocean illustrated by the Baxs proxy, Deep-Sea Res.
349 Pt. I, 52, 355–370, <https://doi.org/10.1016/j.dsr.2004.10.002>, 2005.](#)

350 Dehairs, F., R. Chesselet, and J. Jedwab. “Discrete Suspended Particles of Barite and the Barium
351 Cycle in the Open Ocean.” *Earth and Planetary Science Letters* 49, no. 2 (September 1980):
352 528–50. doi:10.1016/0012-821X(80)90094-1.

353 Dehairs, F., S. Jacquet, N. Savoye, B. A. S. Van Mooy, K. O. Buesseler, J. K. B. Bishop, C. H.
354 Lamborg, et al. “Barium in Twilight Zone Suspended Matter as a Potential Proxy for

355 Particulate Organic Carbon Remineralization: Results for the North Pacific.” *Deep Sea*
356 *Research Part II: Topical Studies in Oceanography*, Understanding the Ocean’s Biological
357 Pump:results from VERTIGO, 55, no. 14–15 (juillet 2008): 1673–83.
358 doi:10.1016/j.dsr2.2008.04.020.

359 Dehairs, F., C. E. Lambert, R. Chesselet, and N. Risler. “The Biological Production of Marine
360 Suspended Barite and the Barium Cycle in the Western Mediterranean Sea.”
361 *Biogeochemistry* 4, no. 2 (June 1, 1987): 119–40. doi:10.1007/BF02180151.

362 Dehairs, F., D. Shopova, S. Ober, C. Veth, and L. Goeyens. “Particulate Barium Stocks and
363 Oxygen Consumption in the Southern Ocean Mesopelagic Water Column during Spring and
364 Early Summer: Relationship with Export Production.” *Deep Sea Research Part II: Topical*
365 *Studies in Oceanography* 44, no. 1–2 (1997): 497–516. doi:10.1016/S0967-0645(96)00072-
366 0.

367 Ellison, Eurachem/CITAC Guide CG4, Quantifying Uncertainty in Analytical Measurement.
368 Eds. S.L.R. Ellison, M. Rosslein and A. Williams. Second edition ISBN 0948926 15 5, Pp
369 120, 2000.

370 Giering, Sarah L. C., Richard Sanders, Richard S. Lampitt, Thomas R. Anderson, Christian Tamburini,
371 Mehdi Boutrif, Mikhail V. Zubkov, et al. “Reconciliation of the Carbon Budget in the Ocean’s
372 Twilight Zone.” *Nature* 507, no. 7493 (March 27, 2014): 480–83.

373 Hainbucher, D., A. Rubino, V. Cardin, T. Tanhua, K. Schroeder, and M. Bensi. “Hydrographic
374 Situation during Cruise M84/3 and P414 (spring 2011) in the Mediterranean Sea.” *Ocean*
375 *Sci.* 10, no. 4 (juillet 2014): 669–82. doi:10.5194/os-10-669-2014.

376 Henson, Stephanie A., Richard Sanders, Esben Madsen, Paul J. Morris, Frédéric Le Moigne, and
377 Graham D. Quartly. “A Reduced Estimate of the Strength of the Ocean’s Biological Carbon
378 Pump.” *Geophysical Research Letters* 38, no. 4 (février 2011): L04606.
379 doi:10.1029/2011GL046735.

380 IPCC Working Group 1, 5th Assessment Report (AR5) Climate Change 2013, Published in Jan.
381 2014.

382 [Jacquet S.H.M., Dehairs F., Dumont I., Becquevort S., Cavagna A.-J., Cardinal, D.: Twilight
383 zone organic carbon remineralization in the Polar Front Zone and Subantarctic Zone south
384 of Tasmania, *Deep-Sea Res. Pt. II*, 58, 2222–2234, <https://doi.org/10.1016/j.dsr2.2011.05.029>,
385 \[2011\]\(#\).](#)

386 Jacquet, S. H. M., F. Dehairs, D. Lefèvre, A. J. Cavagna, F. Planchon, U. Christaki, L. Monin, L.
387 André, I. Closset, and D. Cardinal. “Early Spring Mesopelagic Carbon Remineralization and
388 Transfer Efficiency in the Naturally Iron-Fertilized Kerguelen Area.” *Biogeosciences* 12, no.
389 6 (March 17, 2015): 1713–31. doi:10.5194/bg-12-1713-2015.

390 Jacquet, S. H. M., F. Dehairs, N. Savoye, I. Obernosterer, U. Christaki, C. Monnin, and D.
391 Cardinal. “Mesopelagic Organic Carbon Remineralization in the Kerguelen Plateau Region
392 Tracked by Biogenic Particulate Ba.” *Deep Sea Research Part II: Topical Studies in
393 Oceanography*, KEOPS: Kerguelen Ocean and Plateau compared Study, 55, no. 5–7 (March
394 2008): 868–79. doi:10.1016/j.dsr2.2007.12.038, [2008b](#)

395 Jacquet, S. H. M., J. Henjes, F. Dehairs, A. Worobiec, N. Savoye, and D. Cardinal. “Particulate
396 Ba-Barite and Acantharians in the Southern Ocean during the European Iron Fertilization

397 Experiment (EIFEX).” *Journal of Geophysical Research* 112, no. G4 (October 23, 2007).
398 doi:10.1029/2006JG000394.

399 Jacquet, S.H.M., C. Monnin, V. Riou, L. Jullion, and T. Tanhua. “A High Resolution and Quasi-
400 Zonal Transect of Dissolved Ba in the Mediterranean Sea.” *Marine Chemistry* 178 (January
401 20, 2016): 1–7. doi:10.1016/j.marchem.2015.12.001.

402 [Jacquet S.H.M., Savoye N., Dehairs F., Strass V.H., Cardinal D.: Mesopelagic carbon remineralization](#)
403 [during the European Iron Fertilization Experiment, *Global Biogeochem. Cy.*, 22, 1–9,](#)
404 <https://doi.org/10.1029/2006GB002902>, 2008a.

405 Jullion, L., S. H. M. Jacquet, and T. Tanhua. “Untangling Biogeochemical Processes from the
406 Impact of Ocean Circulation: First Insight on the Mediterranean Dissolved Barium
407 Dynamics.” *Global Biogeochemical Cycles* 31, no. 8 (2017): 1256–70.
408 doi:10.1002/2016GB005489.

409 Kirchman DL (1993) Leucine incorporation as a measure of biomass production by heterotrophic
410 bacteria. In: Kemp PF, Sherr BF, Sherr EB, Cole JJ (eds) *Handbooks of methods in aquatic*
411 *microbial ecology*. Lewis Publishers, Boca Raton, Ann Arbor, London, Tokyo, p 509–512

412 Lemaitre, N., H. Planquette, F. Planchon, G. Sarthou, S. Jacquet, M. I. García-Ibáñez, A.
413 Gourain, et al. “Particulate Barium Tracing of Significant Mesopelagic Carbon
414 Remineralisation in the North Atlantic.” *Biogeosciences* 15, no. 8 (2018): 2289–2307.
415 doi:10.5194/bg-15-2289-2018.

416 Malanotte-Rizzoli, P., V. Artale, G. L. Borzelli-Eusebi, S. Brenner, A. Crise, M. Gacic, N. Kress,
417 et al. “Physical Forcing and Physical/biochemical Variability of the Mediterranean Sea: A

418 Review of Unresolved Issues and Directions for Future Research.” *Ocean Science* 10, no. 3
419 (2014): 281–322. doi:10.5194/os-10-281-2014.

420 Martin, John H., George A. Knauer, David M. Karl, and William W. Broenkow. “VERTEX:
421 Carbon Cycling in the Northeast Pacific.” *Deep Sea Research Part A. Oceanographic
422 Research Papers* 34, no. 2 (1987): 267–85. doi:http://dx.doi.org/10.1016/0198-
423 0149(87)90086-0.

424 [Martinez-Ruiz, Francisca, Fadwa Jroundi, Adina Paytan, Isabel Guerra-Tschuschke, María del
425 Mar Abad, and María Teresa González-Muñoz. “Barium Bioaccumulation by Bacterial
426 Biofilms and Implications for Ba Cycling and Use of Ba Proxies.” *Nature Communications*
427 9, no. 1 \(April 24, 2018\): 1619. doi:10.1038/s41467-018-04069-z.](#)

428 [Martinez-Ruiz, F., A. Paytan, M.T. Gonzalez-Muñoz, F. Jroundi, M.M. Abad, P.J. Lam, J.K.B.
429 Bishop, T.J. Horner, P.L. Morton, and M. Kastner. “Barite Formation in the Ocean: Origin
430 of Amorphous and Crystalline Precipitates.” *Chemical Geology* 511 \(April 20, 2019\): 441–
431 51. doi:10.1016/j.chemgeo.2018.09.011.](#)

432 Ramondenc, Simon, Goutx Madeleine, Fabien Lombard, Chiara Santinelli, Lars Stemmann,
433 Gabriel Gorsky, and Lionel Guidi. “An Initial Carbon Export Assessment in the
434 Mediterranean Sea Based on Drifting Sediment Traps and the Underwater Vision Profiler
435 Data Sets.” *Deep Sea Research Part I: Oceanographic Research Papers* 117 (November
436 2016): 107–19. doi:10.1016/j.dsr.2016.08.015.

437 Sanchez-Vidal, A., R. W. Collier, A. Calafat, J. Fabres, and M. Canals (2005), Particulate barium
438 fluxes on the continental margin: A study from the Alboran Sea (Western Mediterranean),
439 *Mar. Chem.*, 93, 105–117.

440 Santinelli, Chiara, Luciano Nannicini, and Alfredo Seritti. “DOC Dynamics in the Meso and Bathypelagic
441 Layers of the Mediterranean Sea.” *Deep Sea Research Part II: Topical Studies in Oceanography,*
442 *Ecological and Biogeochemical Interactions in the Dark Ocean*, 57, no. 16 (août 2010): 1446–59.
443 doi:10.1016/j.dsr2.2010.02.014.

444 Siegel DA, Buesseler KO, Behrenfeld MJ, Benitez-Nelson CR, Boss E, Brzezinski MA, Burd A, Carlson
445 CA, D'Asaro EA, Doney SC, Perry MJ, Stanley RHR and Steinberg DK (2016) Prediction of the
446 Export and Fate of Global Ocean Net Primary Production: The EXPORTS Science Plan. *Front. Mar.*
447 *Sci.* 3:22. doi: 10.3389/fmars.2016.00022

448 Simon M, Azam F (1989) Protein content and protein synthesis rates of planktonic marine
449 bacteria. *Mar Ecol Prog Ser* 51:201–213

450 Shopova, D., F. Dehairs, and W. Baeyens. “A Simple Model of Biogeochemical Element
451 Distribution in the Oceanic Water Column.” *Journal of Marine Systems* 6, no. 4 (juin 1995):
452 331–44. doi:10.1016/0924-7963(94)00032-7.

453 Speicher, E. A., S. B. Moran, A. B. Burd, R. Delfanti, H. Kaberi, R. P. Kelly, C. Papucci, et al.
454 “Particulate Organic Carbon Export Fluxes and Size-Fractionated POC/234Th Ratios in the
455 Ligurian, Tyrrhenian and Aegean Seas.” *Deep Sea Research Part I: Oceanographic*
456 *Research Papers* 53, no. 11 (2006): 1810–30.
457 doi:http://dx.doi.org/10.1016/j.dsr.2006.08.005.

458 Sternberg, E., C. Jeandel, E. Robin, and M. Souhaut. “Seasonal Cycle of Suspended Barite in the
459 Mediterranean Sea.” *Geochimica et Cosmochimica Acta* 72, no. 16 (2008): 4020–34.
460 doi:<https://doi.org/10.1016/j.gca.2008.05.043>.

461 Tamburini C, Canals M, Durieu de Madron X, Houpert L, Lefèvre D, Martini S, D’Ortenzio F,
462 Robert A, Testor P, and the ANTARES collaboration (2013) Deep-sea bioluminescence
463 blooms after dense water formation at the ocean surface. *PLoS One* 8:e67523

464 Tamburini C, Garcin J, Ragot M, Bianchi A (2002) Biopolymer hydrolysis and bacterial
465 production under ambient hydrostatic pressure through a 2000 m water column in the NW
466 Mediterranean. *Deep Res II* 49:2109–2123

467 Taylor, S.R., McLennan, S.M.: The continental crust: its composition and evolution, Blackwell
468 Scientific Publications, 312pp, 1985.

469

470

471

472

473

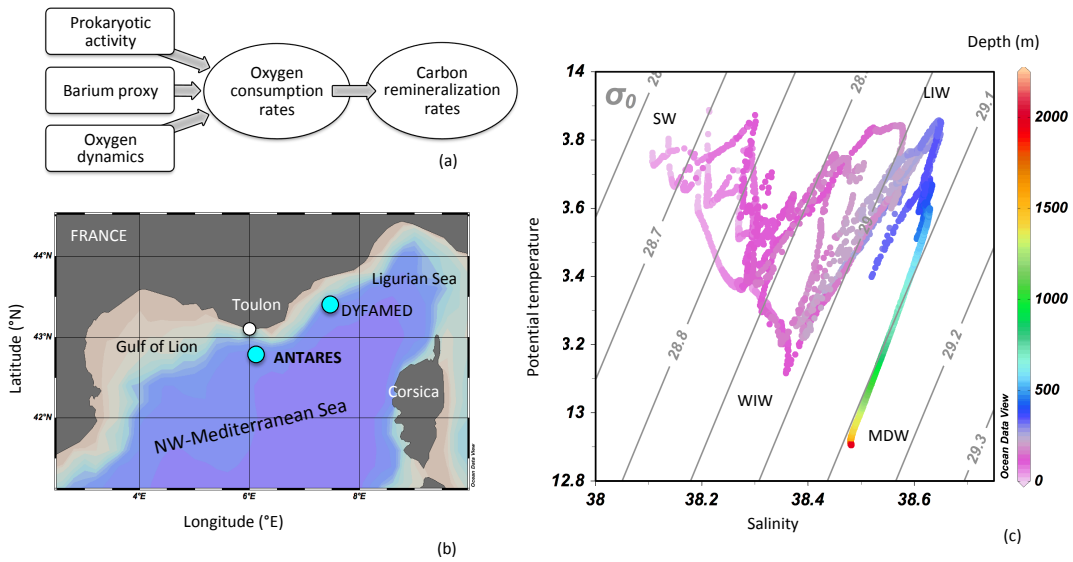
474

475

476

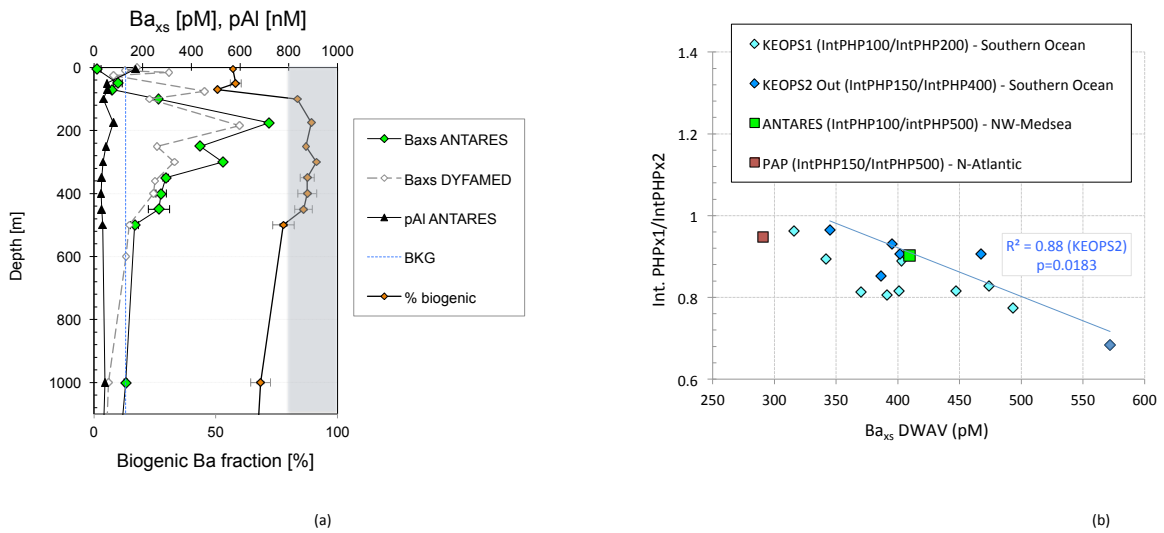
477

478 FIGURE 1



479

480 FIGURE 2



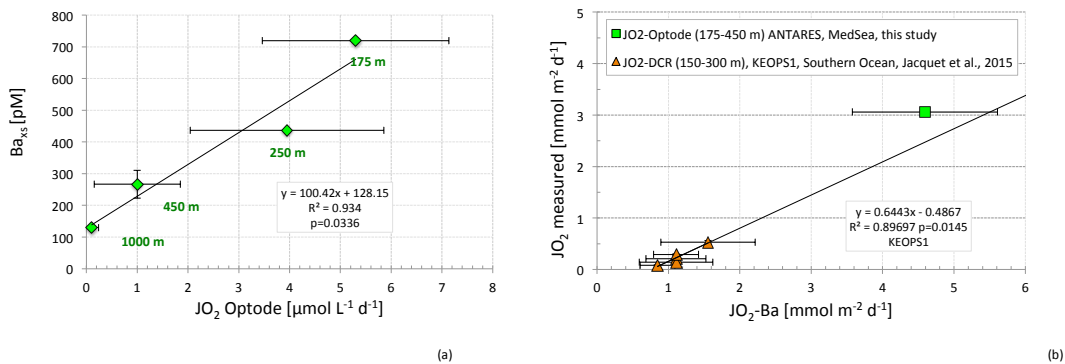
481

482

483

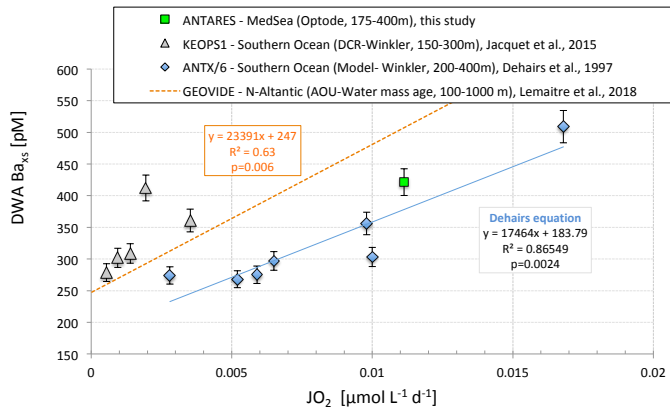
484 FIGURE 3

485



(a)

(b)



(c)

486

487

488